

Cracking mechanisms of diagonal-shear failure monitored and identified by AE-SiGMA Analysis

K. Ohno, S. Shimozono & M. Ohtsu

Graduate School of Science and Technology, Kumamoto University

ABSTRACT: The maintenance of concrete structures has become a serious problem, because concrete is to be realized as no longer maintenance-free. Recently, diagonal shear failure of concrete structures draws a great attention because of disastrous damages due to earthquakes. Accordingly, structural monitoring and assessment of failure or damage by nondestructive evaluation (NDE) is in remarkable demand. Acoustic emission (AE) is known to be promising for NDE of concrete structures for diagnostics and health monitoring. It is known that fracture mechanisms are identified by AE wave form analysis. As a quantitative waveform analysis of AE signals, SiGMA (simplified Green's functions for moment tensor analysis) procedure has been developed. Based on the moment tensor analysis, crack location, crack type and crack orientation are readily identified. In the present study, diagonal shear failure in reinforced concrete (RC) beams is investigated, applying the SiGMA analysis. Thus, cracking mechanisms are clarified and an application to structural monitoring is discussed.

1 INTRODUCTION

The mechanisms of diagonal shear failure in reinforced concrete (RC) beams have not been completely clarified yet. The failure type of RC beams depends on the ratio of the shear span to the effective depth (a/d). Generally, in the case where the ratio a/d is large than 3.0, diagonal tensile failure occurs in RC beams as generated cracks lead to the ultimate state in the beams.

AE method is one of nondestructive testings for concrete structures for diagnostics and health monitoring. AE phenomena are theoretically defined as elastic waves emitted due to microfracturing or faulting in a solid. Emitted AE waves of feeble amplitudes are characterized by high-frequency components in the ultrasonic range. Because the detected AE waves associated with the sources, information on the source mechanisms are contained in AE waves. As a quantitative inverse analysis of AE waveforms, SiGMA (simplified Green's functions for moment tensor analysis) procedure has been developed (Ohtsu, 1991). Kinematics of AE source, such as crack location, crack type and crack orientation can be analyzed from recorded AE waveforms.

In the present paper, AE method is applied to diagonal shear failure of RC beams. Prior to bending tests of RC beams, theoretical waveforms were calculated in order to determine proper location of AE sensors. Theoretical waveforms were synthesized by

applying the dislocation model and Green's functions in a half space. Then, the mechanisms of internal cracks due to bending fracture were identified by SiGMA analysis. In three-dimensional (3D) massive body of concrete, the applicability of SiGMA analysis has been confirmed (Ohtsu et al., 1998). Here AE sources due to diagonal shear failure are located and classified of crack type from recorded AE waveforms.

2 SiGMA ANALYSIS

2.1 Theory of Moment Tensor

As formulated in the generalized theory (Ohtsu and Ono, 1984), AE waves are elastic waves generated by dynamic-crack (dislocation) motions inside a solid. As AE waves are generated by microcracks, wave motion $u_i(\mathbf{x}, t)$ can be represented,

$$u_i(x, t) = \int_F T_{ik}(x, x', t) * b_k(x', x) dS, \quad (1)$$

where T_{ik} is Green's function of the second kind and $*$ denotes the convolution integral. b_k is the crack motion.

In case of an isotropic elasticity,

$$T_{ik} = \lambda G_{ij, j} n_k + \mu G_{ik, j} n_j + \mu G_{ij, k} n_j, \quad (2)$$

where λ and μ are Lamé constants. G_{ik} are the Green's functions. n_k is the crack normal vector.

Substituting Equation 2 into Equation 1, and introducing moment tensor, M_{pq} , $u_i(\mathbf{x},t)$ can be represented as,

$$u_i(x,t) = \int_F T_{ik}(x,x',t) * b_k(x',t) dS$$

$$= G_{ip,q}(x,x',t) M_{pq} * S(t) \quad (3)$$

Here, $G_{ip,q}(\mathbf{x},\mathbf{x}',t)$ are spatial derivative of Green's functions and $S(t)$ represents the source kinetics (the source-time function). Inverse solutions of Equation 3 contain two-fold information of the sources. Source kinetics are determined from the source-time function $S(t)$ by a deconvolution procedure. Source kinematics are represented by the moment tensor, M_{pq} . In order to perform the deconvolution and to determine the moment tensor, the spatial derivatives of Green's functions or the displacement fields of Green's functions due to the equivalent force models are inherently required. Consequently, based on the far-field term of the P-wave, a simplified procedure was developed (Ohtsu, 1991). The procedure is implemented as the SiGMA (Simplified Green's functions for Moment Tensor Analysis) code.

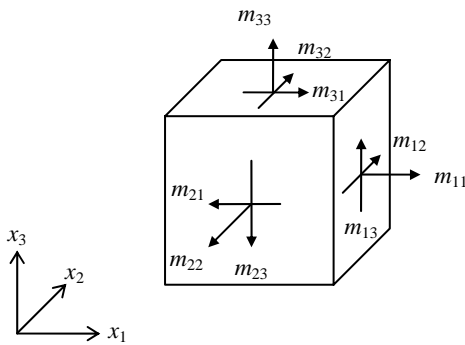
Mathematically, the moment tensor in Equation 3 is defined by the tensor product of the elastic constants, the normal vector \mathbf{n} to the crack surface and the crack-motion (dislocation or Burgers) vector \mathbf{l} .

$$M_{pq} = C_{pqij} l_i n_j \Delta V \quad (4)$$

The elastic constants C_{pqij} have a physical unit of $[N/m^2]$ and the crack volume ΔV has a unit of $[m^3]$. The moment tensor has the physical unit of a moment, $[Nm]$. This is the reason why the tensor M_{pq} was named the moment tensor. The moment tensor is a symmetric second-rank tensor and is comparable to the elastic stress in elasticity as,

$$[M_{pq}] = \begin{bmatrix} m_{11} & m_{12} & m_{13} \\ m_{12} & m_{22} & m_{23} \\ m_{13} & m_{23} & m_{33} \end{bmatrix} \Delta V \quad (5)$$

All elements of the moment tensor are illustrated in Figure 1. In a similar manner to stress, diagonal



element represent normal components and off-diagonal elements are shown as tangential or shear components.

Figure 1. Elements of the moment tensor.

2.2 Equivalent Force Models

AE sources can be represented by equivalent force models, such as a monopole force, a dipole force and a couple force. Relations among crack (dislocation) models, equivalent force models and moment tensors are straightforward. From Equation 4, in an isotropic material we have

$$M_{pq} = (\lambda l_k n_k \delta_{pq} + \mu l_p n_q + \mu l_q n_p) \Delta V \quad (6)$$

In the case that a tensile crack occurs on a crack surface parallel to the x-y plane and opens in the z-direction as shown Figure 2, the normal vector $\mathbf{n} = (0,0,1)$ and the crack vector $\mathbf{l} = (0,0,1)$. Substituting these into Equation 6, the moment tensor becomes,

$$M_{pq} = \begin{bmatrix} \lambda & 0 & 0 \\ 0 & \lambda & 0 \\ 0 & 0 & \lambda + 2\mu \end{bmatrix} \Delta V \quad (7)$$

Only diagonal elements are obtained, which are shown in Figure 2(b). Replacing these diagonal elements as dipole forces, three dipole-forces are illustrated in Figure 2(c). This implies that combination of three dipoles is necessary and sufficient to model a tensile crack.

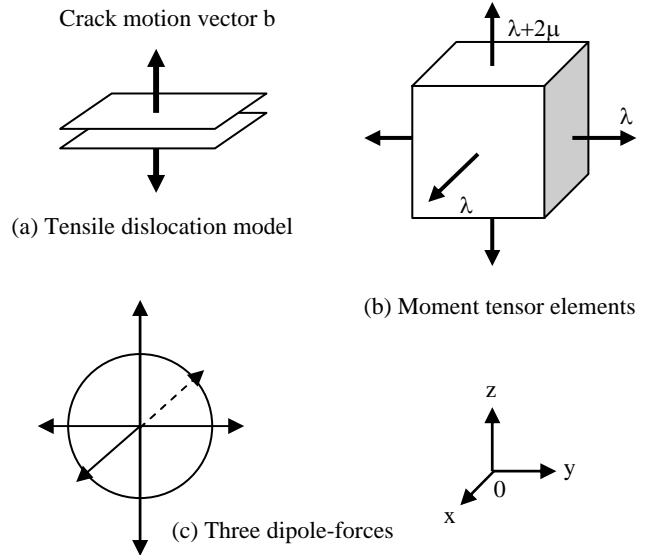


Figure 2. (a) Tensile dislocation model, (b) related moment tensor elements and (c) three dipole-force

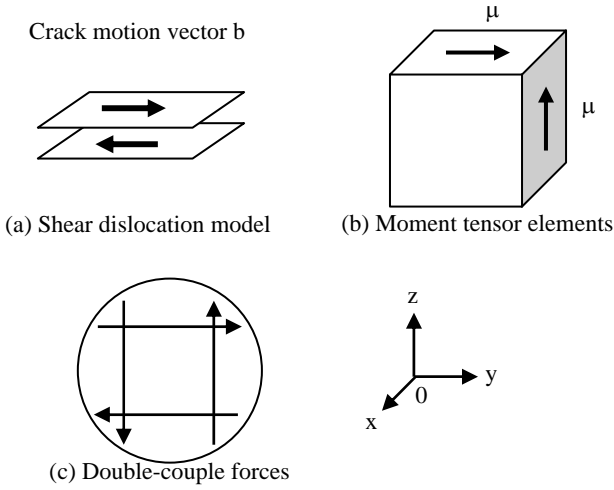


Figure 3. (a) Shear dislocation model, (b) related moment tensor elements and (c) double-couple forces.

In Figure 3, the case of a shear crack parallel to the x-y plane is shown with the normal vector $\mathbf{n} = (0,0,1)$. Shear motion occurs in the y-direction with the crack vector $\mathbf{l} = (0,1,0)$. From Equation 6, we have,

$$M_{pq} = \begin{bmatrix} 0 & 0 & 0 \\ 0 & 0 & \mu \Delta V \\ 0 & \mu & 0 \end{bmatrix} \quad (8)$$

As seen in Figure 3(c), the double-couple force model is comparable to off-diagonal elements of the moment tensor in Equation 8.

2.3 SiGMA Code

Taking into account only P-wave motion of the far field ($1/R$ term) and considering the effect of reflection at the surface, the amplitude of the first motion is derived from Equation 3. The reflection coefficient $\text{Ref}(\mathbf{t}, \mathbf{r})$ is obtained as \mathbf{t} is the direction of sensor sensitivity and \mathbf{r} is the direction vector of distance R from the source to the observation point, as $\mathbf{r} = (r_1, r_2, r_3)$. The time function is neglected in Equation 3, and the amplitude of the first motion $A(\mathbf{x})$ is represented,

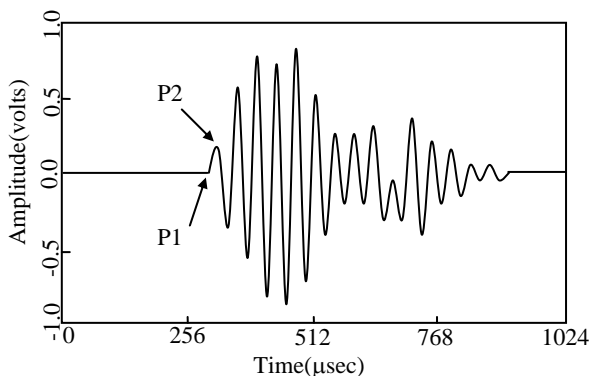


Figure 4. Detected AE waveform.

$$A(\mathbf{x}) = C_s \cdot \frac{\text{Ref}(\mathbf{t}, \mathbf{r})}{R} \cdot (r_1, r_2, r_3) \begin{bmatrix} m_{11} & m_{12} & m_{13} \\ m_{12} & m_{22} & m_{23} \\ m_{13} & m_{23} & m_{33} \end{bmatrix} \begin{bmatrix} r_1 \\ r_2 \\ r_3 \end{bmatrix} \quad (9)$$

where C_s is the calibration coefficient of the sensor sensitivity and material constants. Since the moment tensor is a symmetric tensor of the 2nd rank, the number of independent elements is six. These are represented in Equation 9 as m_{11} , m_{12} , m_{13} , m_{22} , m_{23} , and m_{33} .

These can be determined from the observation of AE waves at more than six sensor locations. In the SiGMA procedure, two parameters of the arrival time (P1) and the amplitude of the first motion (P2) are visually determined from AE waveform as shown in Figure 4. In the location procedure, the source (crack) location \mathbf{x}' in Equation 3 is determined from the arrival time differences t_i between the observation points \mathbf{x}_i and \mathbf{x}_{i+1} , by solving equations,

$$R_i - R_{i+1} = |\mathbf{x}_i - \mathbf{y}| - |\mathbf{x}_{i+1} - \mathbf{y}| = v_p t_i \quad (10)$$

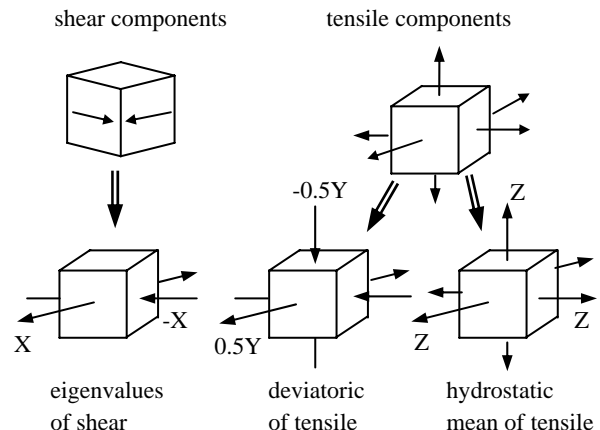
Here v_p is the velocity of P-wave.

After solving Equation 10, the reflection coefficient $\text{Ref}(\mathbf{t}, \mathbf{r})$, the distance R , and direction vector \mathbf{r} are readily obtained to solve Equation 9. The amplitude of the first motions P2 in Figure 4 at more than six channels are substituted into Equation 9, and all the elements of the moment tensor are determined. Since the SiGMA code requires only relative values of the moment tensor elements, the relative coefficients C_s are sufficient.

2.4 Eigenvalue Analysis of the Moment Tensor

In order to classify a crack into a tensile or shear type, a unified decomposition of the eigenvalues of the moment tensor was developed (Ohtsu, 1991). In general, crack motion on the crack surface consists of slip motion (shear components) and crack-opening motion (tensile components), as illustrated in Figure 5.

Figure 5. Unified decomposition of eigenvalues of the moment



tensor.

Thus, it is assumed that the eigenvalues of the moment tensor are the combination of those of a shear crack and of a tensile crack, as the principal axes are identical. Then, the eigenvalues are decomposed uniquely into those of a shear crack, the deviatoric components of a tensile crack and the isotropic (hydrostatic mean) components of a tensile crack. In Figure 5, the ratio X represents the contribution of a shear crack. In that case, three eigenvalues of a shear crack become $X, 0, -X$. Setting the ratio of the maximum deviatoric tensile component as Y and the isotropic tensile component as Z , three eigenvalues of a tensile crack are denoted as $Y+Z, -Y/2+Z$, and $-Y/2+Z$. Eventually the decomposition leads to relations,

$$1.0 = X + Y + Z,$$

the intermediate eigenvalue/the maximum eigenvalue

$$= 0 - Y/2 + Z,$$

the minimum eigenvalue/the maximum eigenvalue

$$= -X - Y/2 + Z.$$

(11)

It should be pointed out that the ratio X becomes larger than 1.0 in the case that both the ratios Y and Z are negative (Suaris and van Mier, 1995). The case happens only if the scalar product $l_k n_k$ is negative, because the eigenvalues are determined from relative tensor components. Making the scalar product positive and re-computing Equation 11, the three ratios are reasonably determined. Hereinafter, the ratio X is called the shear ratio.

In the present SiGMA code, AE sources with shear ratios less than 40%, are classified as tensile cracks. The sources with $X > 60\%$ are classified as shear cracks. In between 40% and 60%, the cracks are referred to as mixed-mode.

From the eigenvalue analysis, three eigenvectors $e1, e2, e3$ are also obtained. Theoretically, these are derived as,

$$\begin{aligned} e1 &= l + n \\ e2 &= l \times n \\ e3 &= l - n \end{aligned} \quad (12)$$

Here \times denotes the vector product, and the vectors l and n are interchangeable. In the case of a tensile crack, the vector l is parallel to the vector n . Thus, the vector $e1$ could give the direction of crack-opening, while the sum $e1+e3$ and the difference $e1-e3$ give the two vectors l and n for a shear crack.

To locate AE sources, at least 5-channel system is necessary for 3-D analysis. Since 6-channel system is the minimum requirement for the moment tensor,

6-channel system is required for the SiGMA-3D analysis.

3 THEORETICAL AE WAVEFORMS

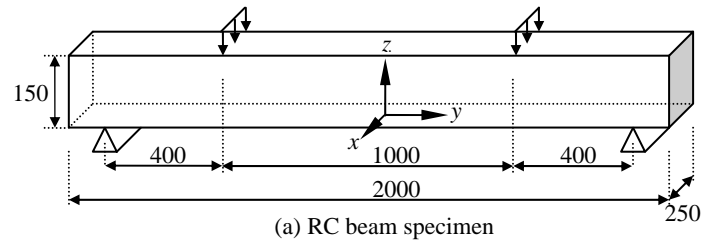
3.1 AE Source Models

In order to determine AE sensor locations, the theoretical waves are analyzed. Based on the location and moment tensors, elastic waves due to a tensile crack, an in-plane shear crack and an out-of-plane shear crack in a half-space were calculated theoretically at the sensor locations. The basic code for computation was already published (Ohtsu & Ono, 1984, Ohtsu & Ono, 1988, Ohtsu & Ohno & Hamstad, 2005).

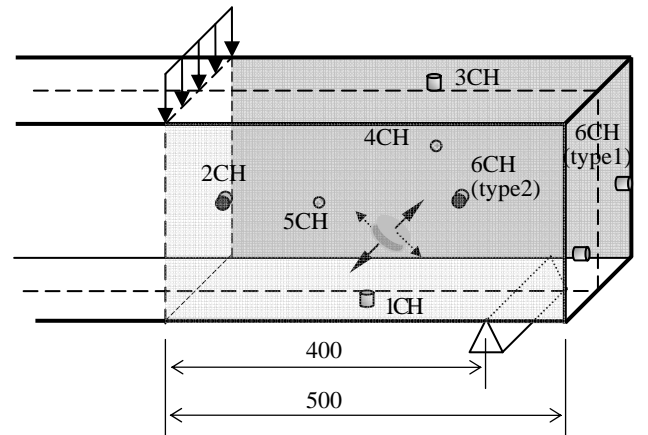
RC beams of dimensions 250mm \times 150mm \times 2000mm with 400mm shear span were tested. The compressive strength and the tensile strength of concrete at 28-day standard curing were 29.7 MPa and 3.03 MPa, respectively. The velocity of P-wave was 4230 m/s and the modulus of elasticity was 28.2 GPa. Poisson's ratio was 0.2. P-wave velocity and Poisson's ratio were applied to SiGMA analysis.

At the origin of the coordinates system, three cracks were considered as source models. Cracks that are a tensile crack, an in-plane shear crack and an out-of-plane shear crack are assumed to be generated in the shear span (Figure 6).

A tensile crack, of which the normal vector $n = (0, 1/\sqrt{2}, 1/\sqrt{2})$ and the crack vector $l = (0, 1/\sqrt{2}, 1/\sqrt{2})$, occurs inclined 45° to y-axis. The moment tensor of a tensile crack is represented as,



(a) RC beam specimen



(b) AE sensor location

$$M_{pq} = \begin{bmatrix} \lambda & 0 & 0 \\ 0 & \lambda + \mu & \mu \\ 0 & \mu & \lambda + \mu \end{bmatrix} \Delta V. \quad (13)$$

Figure 6. (a) RC beam specimen, (b) AE sensor location (unit:mm)

Table 1. The coordinate of AE sensor location

Type1	x(m)	y(m)	z(m)
1CH	0.030	0.700	0.000
2CH	0.075	0.600	0.120
3CH	0.000	0.800	0.250
4CH	-0.075	0.750	0.200
5CH	-0.075	0.650	0.050
6CH	-0.025	1.000	0.125
Type2	x(m)	y(m)	z(m)
1CH	0.030	0.700	0.000
2CH	0.075	0.600	0.120
3CH	0.000	0.800	0.250
4CH	-0.075	0.750	0.200
5CH	-0.075	0.650	0.050
6CH	0.075	0.900	0.105

The moment tensor of an in-plane shear crack model the crack vector of which is $\mathbf{l} = (0, -1/\sqrt{2}, 1/\sqrt{2})$ is represented as,

$$M_{pq} = \begin{bmatrix} 0 & 0 & 0 \\ 0 & -\mu & 0 \\ 0 & 0 & \mu \end{bmatrix} \Delta V \quad (14)$$

The moment tensor of an out-of-plane shear crack model is obtained as setting $\mathbf{l} = (1, 0, 0)$

$$M_{pq} = \begin{bmatrix} 0 & \frac{1}{\sqrt{2}}\mu & \frac{1}{\sqrt{2}}\mu \\ \frac{1}{\sqrt{2}}\mu & 0 & 0 \\ \frac{1}{\sqrt{2}}\mu & 0 & 0 \end{bmatrix} \Delta V \quad (15)$$

Since six sensors were assumed as one group, two types of sensor sets were located in the specimen. The coordinate of these AE sensor locations are shown in Figure 6 and Table 1. The origin of X and Y coordinates is set at the center of the specimen and Z origin is at the bottom in the specimen. Three types of cracks were modeled in the shear span (Figure 6(b)). At five locations in the shear span, these cracks are nucleated for each crack model. Elastic waves generated due to three types of crack models in the specimen were detected at the surface of specimen by two types of sensor locations.

3.2 Results of SiGMA analysis

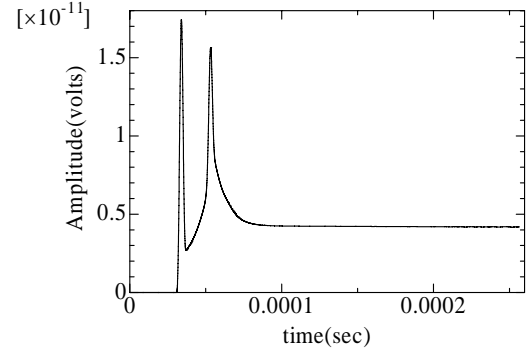
Table 2. Results of SiGMA analysis

Crack mode	Tensile-mode	Mixed-mode	Shear-mode
------------	--------------	------------	------------

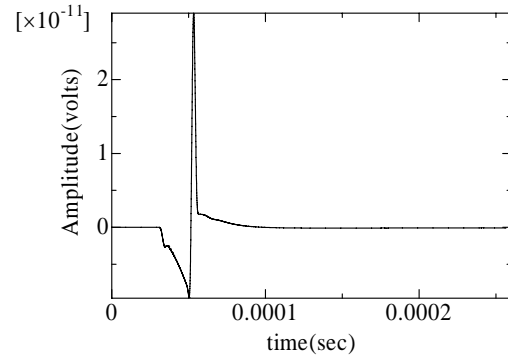
Assumed crack	Results of Type1		
Tensile	1	1	3
In-plane-Shear	3	1	1
Out-of-plane-Shear	2	1	2
Assumed crack	Results of Type 2		
Tensile	1	4	0
In-plane-Shear	2	0	3
Out-of-plane-Shear	3	0	2

In Figure 7, examples of waveforms computed are given. Here, the rise time of the source-time function was set to 7 μ sec. The SiGMA analysis was applied to these theoretical waves.

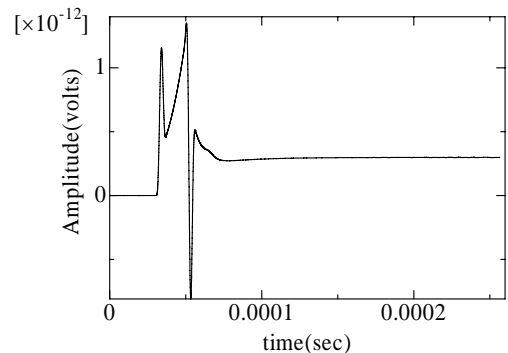
Results are given in Table 2. In the both types, location errors between the crack model and the results of SiGMA analysis do not exist. From the number of classified cracks, it is found that the difference of results between Type 1 and Type 2 does not appear clearly.



(a) Detected AE waveform due to a tensile crack



(b) Detected AE waveform due to an in-plane shear crack



(c) Detected AE waveform due to an out-of-plane shear crack

Figure 7. Example of theoretical waveforms

4 BENDING TEST OF RC BEAM

4.1 Experimental Procedure

Table 3. Mix proportion and properties of concrete.

Weight per unit volume (kg/m ³)				
W/C (%)	Water	Cement	Fine aggregate	Coarse aggregate
55	175	318	717	1178

Admixture (cc)	Slump (cm)	Air (%)	Maximum gravel size (mm)
132	8	6.0	20

The bending test was carried out in RC beam specimens in the laboratory. The specified mix of concrete is shown in Table 3. The effective depth of reinforcing bar is 203.5 mm and shear span is 400 mm ($a/d=1.97$). AE activities were detected by AE sensors of 150 kHz resonance (R15, PAC) and the sampling frequency for recording waveforms is 1 MHz (DiSP, PAC). AE hits were amplified with 40 dB gain in a pre-amplifier and 20 dB gain in a main amplifier.

Based on results of AE source models, AE sensors were arranged, following type 1 and type 2. To detect as many as possible of AE events due to cracks, 8-channel system extending type 1 and type 2 were employed for AE measurement. The tested RC beam and AE sensor configuration are shown in Figure 6 and Figure 8. To monitor diagonal shear failure in the RC beam with AE sensors, stirrups were arranged in a half portion of the specimen. 8 AE sensors covered the whole area of the shear span without stirrups. For other measurements, displacements on two sides were measured with displacement-transducers.

4.2 Results of AE Parameter Analysis

In the bending test, the ultimate load of the RC beam was 96.1 kN. Load and displacement during the test are shown in Figure 9. The displacement varied linearly with stress. As the load increased, the

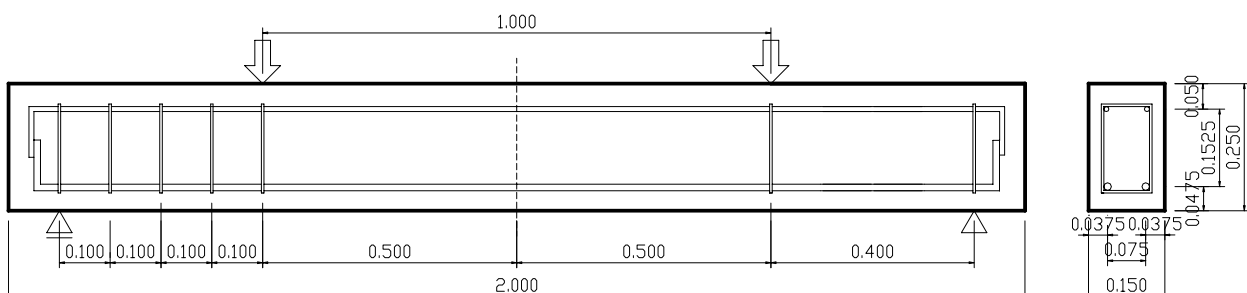
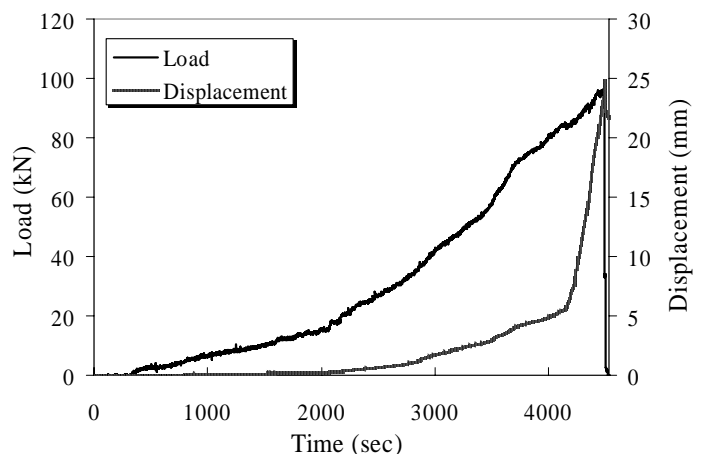
number of AE hits increased and the hits were observed frequently near the ultimate load (Figure 10). The similar process of fracture of the asbestos-cement pipe samples is reported in the previous paper (Suzuki et al., 2006).

Figure 8. Sectional view of the specimen (unit:m).

The flexural crack was observed in middle of the specimen visually at about 46.0 kN. After the occurrence of these cracks, the number of AE hits increased. The shear cracks were observed in shear span at about 84.8 kN.

AE parameter analysis can classify easily crack into two types of tensile mode and shear mode (JCMS-III B5706-2003 code). Two AE parameters which are the RA value and the average frequency are applied to classification of cracks generated. The results of AE parameter analysis are shown in Figure 12. AE hits of 69.14 % of total is classified into the tensile mode, the ratio of the shear mode is 30.86 %. Here, paying attention to variation of AE hits, the testing period is divided into three stages. The stage 1 is the period where the number of AE hits is a few until 53 minutes. In stage 2 until 68 minutes, as the load increased, frequent AE generation is observed. In the final stage, the number of AE hits became the largest and the diagonal failure was occurred.

The results of the three stages are summarized in Table 4. It is clearly found that almost over 60 % AE hits were classified into tensile mode. In the stage 2, as the flexural crack was observed in the middle of the specimen, it is thought that the ratio of tensile mode increased. In addition, in the stage 3, as many cracks grew from bottom of specimen to top of specimen in the shear span, it is thought that the ratio of shear mode increased.



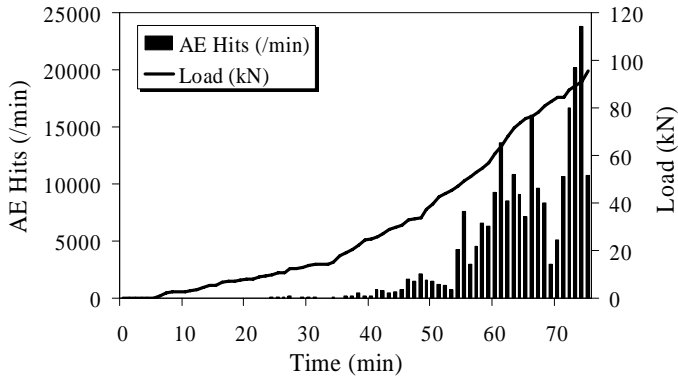


Figure 9. The relation between load and displacement.

Figure 10. AE generation behavior in the bending test.

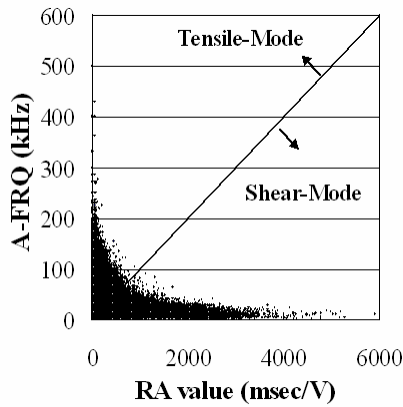


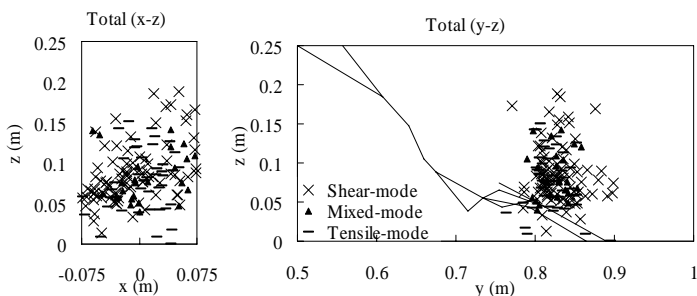
Figure 11. Results of AE parameter analysis

Table 4. The ratio of each mode according to three stages. (AE parameter analysis)

	Tensile-mode	Shear-mode
Stage 1	66.81%	33.19%
Stage 2	75.04%	24.95%
Stage 3	61.40%	38.60%
Total	69.14%	30.86%

4.3 Results of SiGMA analysis

During the bending test, 160 AE events were de-



tected by 8 AE sensors and have been analyzed. Results of the SiGMA analysis are shown in Figure 12.

Kinematics of AE sources are found on the plane of diagonal shear failure. Here, a shear mode is indicated with the cross symbol, a mixed-mode is the triangle symbol and a tensile mode is the bar symbol.

Figure 12. The result of SiGMA analysis.

It is noted that positions of shear cracks are plotted higher than positions of tensile cracks. AE sources of three types are mostly concentrated in around 0.8m from the center of the specimen. In the SiGMA analysis, the event definition time (EDT) is set to 95 μ sec. EDT is used to recognize waveforms occurring within the specified time from the first-hit waveform and to classify them as part of the current event. Therefore, this time might have influence on AE source locations.

The results of three stages are given in Table 5. In all of three stages, shear cracks are distinguished in these events. The results between Table 4 and Table 5 are different. On the other hand, it is realized that the ratio of tensile cracks increases from stage 1 to stage 2. This result is similar to result of AE parameter analysis. From stage 2 to stage 3, the tendency of results of SiGMA analysis is different from results of AE parameter analysis.

The difference between the AE parameter analysis and the SiGMA analysis could result from the fact that AE parameter analysis is carried out based on all AE hits, but SiGMA analysis is applied to only AE events. AE parameter analysis might be included AE events generated in middle of the specimen. This could be the reason why the ratios of the tensile mode are always high in the AE parameter analysis.

Table 5. The ratio of each mode according to three stages. (SiGMA analysis)

	Tensile crack	Mixed-mode	Shear crack
Stage1	20.00%	20.00%	60.00%
Stage2	28.81%	15.25%	55.93%
Stage3	29.73%	16.22%	54.05%
Total	28.75%	15.63%	55.63%

5 CONCLUSION

In this paper, the bending test was carried out in the RC beam specimen and diagonal shear failure process was monitored by AE.

Theoretical waveform analysis was applied to decide the optimal arrangement of AE sensor. As a result, the difference of arrangement of AE sensor between type 1 and type 2 is not clear. Therefore, to detect AE events as many as possible due to cracks, 8-channel system was employed for AE measurement.

It is confirmed that there are three stages in AE generating behaviors. It is found that dominant motions of diagonal shear failure are of the tensile mode by AE parameter analysis. The results of SiGMA analysis, however, dominant source motions in shear span are of the shear mode.

AE parameter analysis carried out based on detected all AE hits, but SiGMA analysis is applied to only AE events. As a result, the ratio of tensile mode is larger than the ratio of shear mode in the AE parameter analysis. This could be the reason why the ratios of the tensile mode are always high in the AE parameter analysis.

REFERENCES

- Ohtsu, M. & Ono, K. 1984. A Generalized Theory of Acoustic Emission and Green's Function in a Half Space. *Journal of AE*. 3(1): 124-133.
- Ohtsu, M. & Ono, K. 1988. AE Source Location and Orientation Determination of Tensile Cracks from Surface Observation: *NDT International*. Vol.21. No.3: 143-150
- Ohtsu, M. 1991. Simplified Moment Tensor Analysis and Unified Decomposition of AE Source: Application to in Situ Hydrofracturing Test. *J.Geophys. Res.*95(2): 6211-6221.
- Ohtsu, M., Okamoto, T. & Yuyama, S. 1998. Moment Tensor Analysis of Acoustic Emission for Cracking Mechanisms in Concrete. *ACI Structural Journal* Vol.95(2): 87-95.
- Ohtsu, M., Ohno, K. & Hamstad, M. 2005. Moment Tensors of In-Plane Waves analyzed by SiGMA-2D. *Journal of AE*. Vol.23: 47-63.
- Suaris, W. & van Mier, J.G.M. 1995. Acoustic Emission Source Characterization in Concrete under Biaxial Loading. *Materials and Structures*, No.28: 444-449
- Suzuki, T., Ohno, K. & Ohtsu, M. 2006. Damage Evaluation of Existing Asbestos-Cement Pipe by Acoustic Emission. *Proceedings of The 18th International Acoustic Emission Symposium*: 257-262.